Spatial colocalization and combined survival benefit of natural killer and CD8 T cells despite profound MHC class I loss in non-small cell lung cancer

Running Title: NK and CD8 T cells antitumor immunity in NSCLC

Remziye E. Wessel,[1] Nardin Ageeb,[2] Joseph M. Obeid,[3] Ileana Mauldin,[4] Kate A. Goundry,[1] Gabriel F. Hanson,[1] Mahdin Hossain,[5] Chad Lehman,[5] Ryan D. Gentzler,[6] Nolan A. Wages,[7] Craig L. Slingluff Jr,[4] Timothy N.J. Bullock,[5,8] Sepideh Dolatshahi,[1,5†] and Michael G. Brown [5,9-11†]

[1]Department of Biomedical Engineering, University of Virginia (UVA) School of Medicine, Charlottesville, Virginia 22908

[2]Department of Biology, UVA, Charlottesville, Virginia 22908

[3]Department of Thoracic Surgery, Temple University Hospital, Philadelphia, Pennsylvania 19140

[4]Department of Surgery, UVA School of Medicine, Charlottesville, Virginia 22908

[5]Beirne B. Carter Center for Immunology Research, UVA School of Medicine, Charlottesville, Virginia 22908

[6]Department of Medicine, Hematology and Oncology, UVA School of Medicine, Charlottesville, Virginia 22908

[7]Department of Biostatistics, Virginia Commonwealth University, Richmond, Virginia 23298-0032

[8]Department of Pathology, UVA School of Medicine, Charlottesville, Virginia 22908

[9]Department of Medicine, Nephrology, UVA School of Medicine, Charlottesville, Virginia 22908

[10]Center for Immunity, Inflammation and Regenerative Medicine, UVA School of Medicine, Charlottesville, Virginia 22908

[11]Department of Microbiology, Immunology and Cancer Biology, UVA School of Medicine, Charlottesville, Virginia 22908

[†]Shared senior authorship.

Keywords: MHC class I, CD8 T cells, natural killer cells, tumor-infiltrating lymphocytes, interferon-gamma, multiplex immunofluorescence, patient survival, tissue micro-array, spatial analysis, systems immunology, intratumor heterogeneity, cell co-localization

Declarations:

Ethics approval and consent to participate – Not applicable.

Consent for publication – Not applicable.

Availability of data and material – Demographics data for Cohort 1 and 2 are included in Supplementary Spreadsheets 1 and 2, respectively. Algorithms developed for this study (O-PLSDA and cell neighborhood scoring) are available on GitHub (https://github.com/Dolatshahi-Lab). Quantitative IHC and mIF data are available as Supplementary Spreadsheets 3-4. IHC and mIF images will be made available by the authors upon reasonable request.

Competing interests – CLS - Research support to UVA from Celldex (funding, drug), Merck (funding, drug), Theraclion (device staff support); Funding to UVA from Polynoma for PI role on the MAVIS Clinical Trial; Funding to UVA for roles on Scientific Advisory Boards for Immatics and

CureVac. CLS receives licensing fee payments through the UVA Licensing and Ventures Group for patents for peptides used in cancer vaccines. RDG – Research support to UVA from Pfizer, Amgen, Chugai, Merck, AstraZeneca, Janssen, Daiichi Sankyo, Alliance Foundation, Takeda, ECOG/ACRIN, Jounce Therapeutics, Bristol Myers Squibb, SWOG, Helsinn, Dizal Pharmaceuticals, and Mirati. RDG received payment for service on Scientific Advisory Boards including AstraZeneca, Takeda, Gilead, Janssen, Mirati, Daiichi Sankyo, Sanofi, Oncocyte, Jazz Pharmaceuticals, Blueprint Medicines, and Merus.

Funding – This work was funded by a Cancer Team Science Award from the UVA Comprehensive Cancer Center (TNJB & MGB), and a Collaborative Research Award from the UVA Beirne Carter Center for Immunology Research (TNJB, SD & MGB). The UVA Comprehensive Cancer Center Support Grant (P30CA044579) from the NCI additionally supported work performed by the Biorepository and Tissue Research Facility (BTRF) and Molecular Immunologic and Translational Science (MITS) core facilities. REW and GFH received training support from National Institute of General Medical Sciences of the National Institutes of Health (T32-GM145443). JMO received training support from National Cancer Institute T32 CA163177 and UVA, Department of Surgery. MH received training support through the UVA College Science Scholar Summer Research stipend. CL received training support through the UVA School of Medicine Summer Medical Research Internship Program.

Authors contributions – REW, SD and MGB wrote the manuscript with input from all authors. REW, NA, JMO, IM, KG, CL, RDG, CLS, TNJB, SD and MGB contributed to the conception, design, and development of the project. REW, NA, JMO, IM, KG, GFH, MH, and NW performed experiments and/or analyzed data. All authors approved the final version of the manuscript.

Acknowledgements – This work was presented at the 2023 American Association of Immunologists (AAI) Annual Meeting (Abstract 62.08). We thank Dr. Patcharin Pramoonjago and outstanding technical support from the Biorepository and Tissue Research Facility (BTRF) which is supported by the University of Virginia (UVA) School of Medicine, Research Resource Identifiers (RRID): SCR_022971. This work was also supported by the UVA Molecular Immunologic & Translational Sciences (MITS) core facility and the co-pay by the UVA Cancer Center Support Grant number 2P30CA044579-26.

Authors' information (optional) –

Michael G. Brown – ORCID iD 0000-0003-2872-7685

Timothy N.J. Bullock – ORCID iD 0000-0001-6141-3261

Sepideh Dolatshahi – ORCID iD 0000-0003-0226-0933

Ryan D. Gentzler – ORCID iD 0000-0002-8983-6677

Joseph Obeid – ORCID iD 0000-0002-6111-9289

Craig L. Slingluff – ORCID ID 0000-0002-6664-4373

Remziye E. Wessel – ORCID iD 0000-0002-8596-4700

Gabriel F. Hanson – ORCID iD 0009-0003-0202-062X

List of abbreviations – Central Tumor, CT; Checkpoint Inhibitor Immunotherapy, CPI; Hazards Ratio, HR; Heavy Chain, HC; Interferon gamma, IFNγ; MHC class I, MHC-I; Multiplexed Immunofluorescence, mIF; Natural Killer cell, NK cell; Non-Small Cell Lung Cancer, NSCLC; Squamous Cell Carcinoma, SCC; Orthogonalized Partial Least Squares Discriminant Analysis, OPLSDA; Peripheral Tumor, PT; Variable Importance in Projection, VIP.

Spatial colocalization and combined survival benefit of natural killer and CD8 T cells despite profound MHC class I loss in non-small cell lung cancer

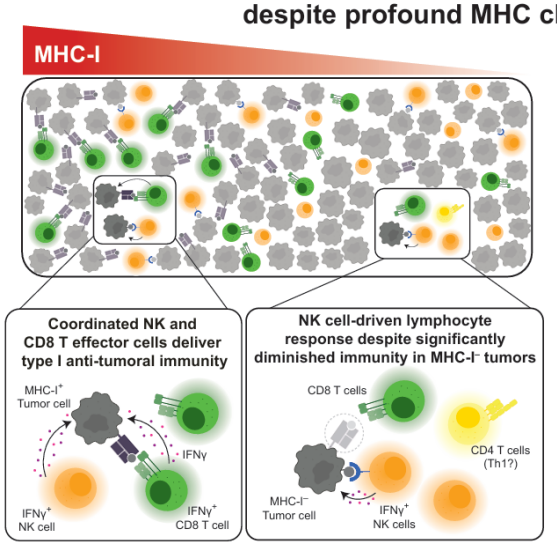

Authors
Remziye E. Wessel, Nardin Ageeb, Joseph M. Obeid, Ileana Mauldin, Kate A. Goundry, Gabriel F. Hanson, Mahdin Hossain, Chad Lehman, Ryan D. Gentzler, Nolan A. Wages, Craig L. Slingluff Jr., Timothy N.J. Bullock, Sepideh Dolatshahi†, and Michael G. Brown†

†Co-correspondence:
sd8us@virginia.edu and mgb4n@virginia.edu

In brief
Tumor-infiltrated natural killer (NK) and CD8 T cells display increased co-localization and evidence of coordinated effector activity in human MHC-I-bearing NSCLC tumors.

Graphical Abstract.

ABSTRACT

Background. MHC class I (MHC-I) loss is frequent in non-small cell lung cancer (NSCLC) rendering tumor cells resistant to T cell lysis. NK cells kill MHC-I-deficient tumor cells, and although previous work indicated their presence at NSCLC margins, they were functionally impaired. Within, we evaluated whether NK cell and CD8 T cell infiltration and activation vary with MHC-I expression. **Methods**. We used single-stain immunohistochemistry (IHC) and Kaplan-Meier analysis to test the effect of NK cell and CD8 T cell infiltration on overall and disease-free survival. To delineate immune covariates of MHC-I-disparate lung cancers, we used multiplexed immunofluorescence (mIF) imaging followed by multivariate statistical modeling. To identify differences in infiltration and intercellular communication between IFNγ-activated and non-activated lymphocytes, we developed a computational pipeline to enumerate single cell neighborhoods from mIF images followed by multivariate discriminant analysis. **Results**. Spatial quantitation of tumor cell MHC-I expression revealed intra- and inter-tumoral heterogeneity, which was associated with the local lymphocyte landscape. IHC analysis revealed that high $CD56^+$ cell numbers in patient

tumors were positively associated with disease-free survival (DFS) (HR=0.58, *p*=0.064) and overall survival (OS) (HR=0.496, *p*=0.041). The OS association strengthened with high counts of both $CD56^+$ and $CD8^+$ cells (HR=0.199, $p<1x10^{-3}$). mIF imaging and multivariate discriminant analysis revealed enrichment of both $CD3^+CD8^+$ T cells and $CD3^-CD56^+$ NK cells in MHC-I-bearing tumors ($p<0.05$). To infer associations of functional cell states and local cell-cell communication, we analyzed spatial single cell neighborhood profiles to delineate the cellular environments of $IFN\gamma^{+/-}$ NK cells and T cells. We discovered that both $IFN\gamma^+$ NK and CD8 T cells were more frequently associated with other $IFN\gamma^+$ lymphocytes in comparison to $IFN\gamma^-$ NK cells and CD8 T cells ($p<1x10^{-30}$). Moreover, $IFN\gamma^+$ lymphocytes were most often found clustered near $MHC\text{-}I^+$ tumor cells. **Conclusions**. Tumor-infiltrating NK cells and CD8 T cells jointly affected control of NSCLC tumor progression. Co-association of NK and CD8 T cells was most evident in MHC-I-bearing tumors, especially in the presence of IFNγ. Frequent co-localization of $IFN\gamma^+$ NK cells with other $IFN\gamma^+$ lymphocytes in near-neighbor analysis suggests NSCLC lymphocyte activation is coordinately regulated.

What is already known on this topic – MHC-I loss occurs frequently in NSCLC and corresponds with waning immunity in the tumor microenvironment (TME). NK cells recognize “missing-self” targets and could be leveraged to target NSCLC tumors with MHC-I loss. While NK cell presence at tumor margins has been documented in NSCLC, they were shown to lose function in this environment.

What this study adds – We developed spatial analysis pipelines leveraging the local heterogeneity of the TME at single cell resolution to test whether NK cells and T cells together contribute antitumoral immunity in NSCLC. We discovered that a high density of tumor-infiltrating NK cells corresponded with DFS, and this association was increased in patients with high coincident CD8 T cells, especially those in central tumor. Intriguingly, both cell types were found clustered

138 together in MHC-I-bearing tumors, especially when both expressed IFNγ, suggesting coordinated
139 lymphocyte activities may enhance immune control of NSCLC.
140
141 **How this study might affect research, practice, or policy –** This study provides a rationale for
142 developing novel immunotherapies that simultaneously increase NK and T cell anti-tumoral im-
143 munity. Associations linking NK cells with patient survival and increased immune effector activity
144 in NSCLC, even in MHC-I-deficient tumors, further highlights the need to devise and deploy NK
145 cell activating strategies which may be highly efficacious in CD8 T cell refractory NSCLC.
146
147

148 **BACKGROUND**

149 Lung cancer is the leading cause of cancer-related death in the United States and globally, and
150 NSCLC accounts for ~85% of all lung cancers.[1 2] Adenocarcinoma (AdenoCA) and squamous
151 cell carcinoma (SCC) together account for ~90% of all NSCLC subtypes.[3 4] Both tumor types are
152 infiltrated by diverse immune cells, including T cells and NK cells with cytokine and cytotoxic
153 effector activity,[5] highlighting the opportunity to harness these cytolytic cells to mediate efficacious
154 control of lung cancer.

155 Tumor cell MHC-I loss to evade recognition by cytotoxic T cells is common in NSCLC,
156 occurring in >30% of human lung cancer cells with >90% having defects of one or more MHC-I
157 antigens or other molecules associated with antigen presentation.[6] This constitutes a logical evo-
158 lutionary step given the propensity of NSCLC to have a large repertoire of antigenic mutations
159 that can be presented to T cells on MHC-I.[7] Despite the frequency of MHC-I loss, its impact on
160 lymphocyte infiltration and patient survival has not been resolved.[8-14]

161 The density of CD8 T cells infiltrating NSCLC tumors has been associated with a favorable
162 prognosis.[15-17] However, assessment of patient risk based on this determination alone is

163 challenging due to factors such as the heterogeneity of intratumoral CD8 T cell infiltrates, the
164 inherent difficulty in reliably sampling and assessing tumor-infiltrating lymphocytes, a plausible
165 role for other immune cells, and because T cell exhaustion can contribute to poor immunological
166 control of lung cancers.[18-20] However, NK cells have been shown to provide protection against
167 hematological malignancies or metastases from primary tumors, yet their antitumor activity has
168 been less evident in solid tumors.[21 22] Given their ability to lyse 'missing-self' targets, NK cells
169 represent a presently unharnessed, yet logical candidate to improve anti-tumor immunity in MHC-
170 I-deficient, T cell-refractory lung tumors.[23]

171 Prior work has shown that NK cells are prevalent in β2-microglobulin (β2m-)deficient
172 NSCLC tumors,[13] but intratumoral NK cells from NSCLC patients were found to have reduced
173 IFNγ production and cytolytic capability compared to circulating NK cells from the same patients.
174 [24] Nonetheless, tumor-infiltrating NK cells activated by cytokines or stimulated via direct recogni-
175 tion of tumor cell expressed ligands of NK activating receptors have been shown to enhance
176 tumor-specific T cells and control of tumor progression, possibly via cytokines to enhance recruit-
177 ment or activation of classical dendritic cells (cDC).[25-30] Understanding NK cell and CD8 T cell
178 interactions supporting the anti-tumor immune response in relation to MHC-I expression in the
179 NSCLC TME is a priority.

180 Hypothesizing that NK cells and CD8 T cells together drive anti-tumor immunity in NSCLC
181 in relation to tumor cell MHC-I expression, we investigated whether tumor-infiltrating NK cells and
182 CD8 T cells were associated with patient survival, and if tumor cell MHC-I expression corre-
183 sponded with variations in lymphocyte presence, activation status, or spatial associations in the
184 NSCLC TME. Our findings suggest that novel strategies designed to leverage both T cells and
185 NK cells in combined immunotherapy may provide enhanced antitumor immunity and increased
186 T cell activation, even in T cell refractory tumors.

187

188 **MATERIALS AND METHODS**

189 **Clinical Patient Enrollment.** Patients with non-small cell lung cancer (NSCLC) seen at the Uni-
190 versity of Virginia between 2011-2014 were enrolled in the clinical Cohort 1 (IRB-HSR#:18346).
191 These participants had a resection at UVA in the years 2000 – 2014 and an available specimen
192 in the UVA Biorepository and Tissue Research Facility. Patients were excluded only if the speci-
193 men was inadequate for testing (i.e., mostly fibrotic or necrotic tissue, or does not contain tumor
194 cells). Clinical staging data is shown for all participants (**Table 1**), including those patients who
195 underwent resection to non-evident disease.

196

197 **Immunohistochemistry.** The AJCC 7th edition was used for clinical and pathological staging. A
198 pathologist outlined tumor areas and margins. Hematoxylin-eosin-stained sections from formalin-
199 fixed, paraffin embedded (FFPE) tissues were used to identify regions of interest for analysis.
200 Central tumor (CT) and peripheral tumor (PT) 1-mm cores, identified by a pathologist, were ex-
201 tracted from the FFPE tissues and used to construct the tissue microarray (TMA) as described.[31]
202 The TMA was incubated with primary antibodies to β2-microglobulin (mAb NAMB-1, kindly pro-
203 vided by Soldano Ferrone), CD3 (mAb Dako, clone 7.2.38), CD8 (clone C8/144B, Dako
204 Carpinteria, CA), CD56 (mAb NCL-L-CD56-1B6, Leica), Granzyme B (ab4059, Abcam), and HLA
205 class I heavy chains (HC) (HC10,[32] kindly provided by Soldano Ferrone). Enzyme-linked second-
206 ary antibodies and 3,3'-diaminobenzidine (Dako) were used to develop the staining. Antibody-
207 stained slides were counterstained with hematoxylin (Dako) and permanently mounted as de-
208 scribed.[31] Images were acquired using a Nikon Digital Sight DS-Fi1 camera (Nikon Corporation,
209 Tokyo, Japan), an Eclipse 400 microscope (Nikon), or a NIS-Elements Viewer version 3.2 (Nikon).
210 Control tissues included tonsil, lymph node, and placenta. Tissues incubated with PBS instead of
211 primary antibody followed by staining with secondary antibody served as negative controls.

212

213 **TMA Immunotyping.** Tumor cell antigen expression was assessed by a pathologist and scored
214 by expression intensity (0=none, 1=mild, 2=strong). Scores from two cores per patient were
215 summed to account for tumor heterogeneity. Automated CD8 counting was performed using a
216 Leica SCN400 Scanner (Leica, Nussloch, Germany) and Digital Imaging Hub (Leica) and vali-
217 dated by manual counting by a pathologist. Immune cell counts were reported as (counts/mm^2).

218

219 **Multiplex immunofluorescence (mIF) imaging and geospatial analysis**. Five µm-thick sec-
220 tions from FFPE resected tumors were analyzed. Human lymph node samples were used as a
221 positive control. mIF was performed according to the manufacturer's protocol using the OPAL
222 Multiplex Manual IHC kit and antigen retrieval (AR) buffers AR6 and AR9 (Akoya Biosciences,
223 Marlborough, Massachusetts, USA) and DIVA Decloaker AR buffer (Biocare Medical, Pacheco,
224 California, USA). Staining sequence, antibodies and AR buffers used are as follow: AR9, CD3
225 (1:100, Cell Marque MRQ-39) Opal520; AR9, CD8 (1:500, clone C8/144B Agilent Technologies,
226 Santa Clara, California, USA) Opal540; AR6, CD56 (1:1000, Cell Marque MRQ-42) Opal570;
227 DIVA, IFNγ (1:1000 NeoBiotechnologies 345 MSM4 P2 IFNG/466) Opal620; AR6, MHC-I
228 (1:15,000 HLA class I heavy chains – HC10,[32] Ferrone Lab) Opal650; AR6 Pan-cytokeratin
229 (panCK) (1:200 MA513203, Invitrogen) Opal690, and AR6, spectral DAPI (Akoya Biosciences)
230 as described.[33]

231 Stained slides were mounted using prolong diamond antifade (Life Technologies, Carls-
232 bad, California, USA) and scanned using the PerkinElmer Vectra 3.0 system and Vectra software
233 (Akoya Biosciences). Regions (3-mm^2) were identified using Phenochart software and tissue im-
234 ages were acquired at 20x magnification with the Vectra 3.0 system. The images were spectrally
235 unmixed using single stain positive control images using InForm software (Akoya Biosciences).
236 A tissue classifier was trained on panCK$^+$ tumor cells and panCK$^-$ stroma followed by cell seg-
237 mentation using HALO software (Indica Labs, Albuquerque, New Mexico, USA). Lymphocyte

238 density (cells/mm^2) was quantified for a given marker within stromal or tumor compartments of
239 each region. To increase statistical power while avoiding size-related representational biases in
240 resected tissues, a patient-agnostic, tissue regional analysis was developed to analyze scanned
241 images of AdenoCA and SCC patient tumor biopsies as independent entities (**supplemental fig-**
242 **ure S1**).

243

244 **Spatial transcriptomics.** The GeoMx Digital Spatial Profiler (DSP) (Nanostring) was used to
245 generate whole transcriptome data for a subset of Cohort 1 patient tumors. FFPE tissue slices
246 (5 μm) were sectioned onto positively charged slides. Regions of interest (ROIs) including at least
247 250 cells were selected based on staining with fluorophore-conjugated mAbs against panCK (AE-
248 1/AE-3, Novus Biologicals), CD8 (C8/144B, Biolegend), and MHC-I HC (HC10, Ferrone Lab).
249 Oligo-tagged profiling reagents were used to interrogate transcript expression within ROIs. Tran-
250 scripts were read using an Illumina Sequencer and gene expression was quantified using the
251 DSP interactive software based on the Whole Transcriptome Atlas.

252 **Survival analyses**. Univariate and multivariate survival analysis was performed using R v.4.2.1.
253 *Kaplan-Meier analysis*. To test the effect of NK and CD8 T cell abundances on OS (the time from
254 resection to death by any cause) and DFS (the time from surgical resection to disease recurrence
255 or death by any cause), patient tumors were stratified at an optimal cut point determined as de-
256 scribed by Contal and O'Quigley [34] based on cell density (cells/mm^2) averaged between CT and
257 PT regions. The effect of MHC-I expression on OS and DFS was similarly determined by com-
258 paring patients with MHC-I expression above or below 60% averaged between CT and PT. Sig-
259 nificance was determined by a log-rank test (p<0.05). Tumors with missing data for any of these
260 markers were excluded from those respective analyses. *Cox proportional hazards modeling*. Pro-
261 portional hazards assumptions were tested using Schoenfeld residual analysis for univariate and
262 multivariate analysis (p<0.01). Multivariate Cox proportional hazards models assessed the

263 relationship between survival endpoints (OS and DFS) and NK cell, CD8 T cell abundances, and
264 MHC-I expression after adjusting for age and sex. Associations were considered significant for
265 two-sided *p* values≤0.05.
266
267 **Cellular neighborhood analysis**. *Custom cell-cell neighborhood scoring algorithm*. Spatial col-
268 ocalizations were determined in Python using single cell 2-dimensional coordinates obtained from
269 HALO. The Euclidian distance between each cell and every other cell on the slide was computed;
270 nearest neighbors were defined as cells with a center-to-center Euclidean distance <30μm (**sup-**
271 **plemental figure S2**). The nearest neighbors of each phenotype were enumerated to yield the
272 neighborhood profile for each cell. *Intercellular K function analyses.* Intercellular geospatial colo-
273 calizations were further analyzed using the Spatstat package in R v.4.2.1.[35] The K function was
274 used to determine the number of nearest neighbors for a given cell type as a function of radius
275 <200μm for each tumor region separately.
276
277 **Multivariate discriminant analyses**. Orthogonalized Partial Least Squares Discriminant Anal-
278 yses (OPLSDA) two-component models were generated in MATLAB (R2022a, MathWorks, Na-
279 tick, MA) using scripts developed in-house.
280 All data input to OPLSDA were log-transformed, centered, and scaled. OPLSDA models
281 were constructed on cell densities per region (cells/mm^2) to discriminate between tumor regions
282 with MHC-I$^+$ tumor cell counts (panCK$^+$MHC-I$^+$) above or below the median for AdenoCA and
283 SCC tumors separately. Cells localized to the tumor or stroma were normalized to their respective
284 compartment areas. Second, OPLSDA models were constructed to discriminate the cellular
285 neighborhood profiles between IFNγ$^{+/-}$ NK cells (CD3$^-$CD56$^+$IFNγ$^{+/-}$) and CD8 T cells
286 (CD3$^+$CD8$^+$IFNγ$^{+/-}$). Prediction accuracy was determined using a random 5-fold cross validation
287 (CV) framework. Significance was determined empirically by comparing the model's CV accuracy

288 against 1000 randomly permuted models.[36 37] Univariate comparisons between model features
289 were conducted using a non-parametric Wilcoxon rank sum test with a Benjamini-Hochberg false
290 discovery rate correction controlled at $p<0.05$.
291

292 **RESULTS**

293 **Patient characteristics**. TMA specimens collected from patients seen at UVA between 2011-
294 2014 were analyzed by single-stain immunohistochemistry (IHC) along with retrospective review
295 of clinical records (IRB-HSR#:18346) (Cohort 1) (**table 1**). Whole tumor resections collected pro-
296 spectively from patients seen at UVA between 2014-2018 were analyzed by mIF (IRB-HSR#
297 13310) (Cohort 2). Two patients in Cohort 2 were treated with Pembrolizumab, one was treated
298 with Atezolizumab, and one was treated with Nivolumab following surgical resection. No patients
299 in Cohort 1 received immunotherapy.
300

301 **Table 1. NSCLC patient characteristics.**

		Cohort 1 (n=151) (Retrospective)			Cohort 2 (n=36) (Prospective)			
Clinical feature *		**AdenoCA** (n=93)	**SCC** (n=58)	**Total**	**AdenoCA** (n=28)	**SCC** (n=8)	**Total**	**Total (Cohort 1 + Cohort 2)**
Biologic sex	Female	49 (53%)	21 (36%)	70 (46%)	20 (71%)	5 (63%)	25 (69%)	95 (51%)
Age in years, mean +/- (range)		67 ± 9 (49-89)	66 ± 9 (38-84)	67 ± 9 (38-89)	66 ± 11 (47-85)	62 ± 12 (55-81)	65 ± 11 (47-85)	66 ± 9 (38-89)
AJCC v7 Stage at excision	Stage I	57 (61%)	36 (62%)	93 (62%)	7 (25%)	0 (0%)	7 (19%)	100 (53%)
	Stage II	20 (22%)	13 (22%)	33 (22%)	10 (36%)	2 (25%)	12 (33%)	45 (24%)
	Stage III	13 (14%)	8 (14%)	21 (14%)	11 (39%)	5 (63%)	16 (44%)	37 (20%)
	Stage IV	3 (3%)	1 (2%)	4 (3%)	0 (0%)	1 (13%)	1 (3%)	5 (3%)
Largest Tumor Diameter* in cm, Mean +/- SD (range)		2.7 ± 1.8 (0.6-12)	3.7 ± 2.4 (0.9-10)	3.1 ± 2.1 (0.6-12)	3.29 ± 1.58 (1.3-6.3)	3.03 ± 1.58 (1.2-5.5)	3.23 ± 1.56 (1.2-6.3)	3.12 ± 1.99 (0.6-12)
Prior chemotherapy		5 (6%)	1 (2%)	6 (4%)	6 (21%)	3 (38%)	9 (25%)	15 (8%)
Treated with anti-PD(L)1 therapy		0 (0%)	0 (0%)	0 (0%)	4 (14%)	0 (0%)	4 (11%)	4 (2%)
* number (%) unless otherwise specified								

302

303 **MHC-I expression variation in human NSCLC is associated with variation in intra-tumoral**
304 **lymphocytes.** To examine MHC-I expression in NSCLC tumors and its relationship with

305 occupation by CD56$^+$ NK cells and CD8 T cells, we performed IHC on Cohort 1 (**table 1**) staining
306 for anti-MHC-I HC, β2m, CD56, and CD8. We observed wide-ranging MHC-I HC expression levels
307 in both AdenoCA and SCC, with >90% MHC-I HC loss in 12% of AdenoCA and 22% of SCC
308 tumors (**figure 1A,D**). At the other extreme, 16 AdenoCAs (17%) and 10 SCCs (17%) had MHC-
309 I expression in 100% of cells. We observed heterogeneity in MHC-I HC expression within each
310 tumor, as CT and PT cores of the same tumor often displayed distinct MHC-I HC expression
311 patterns (**figure 1A,D**). HC10[32] reacts with unfolded HLA-A, -B and -C heavy chains, so it may
312 not identify HLA Class I molecules folded with β2m; thus, we analyzed the correlation of β2m with
313 HLA I HC expression. HLA HC and β2m staining were significantly correlated in AdenoCA and
314 SCC (**figure 1B,E**), suggesting that low HC10 staining may be related to decreased surface ex-
315 pression of folded MHC-I dimers as well. This finding was consistent at the gene expression level
316 (**supplemental figure S3**). Nonetheless, variability in MHC-I HC for each β2m classification sug-
317 gested other regulators of MHC-I expression and/or antigen presentation may have affected
318 MHC-I loss in Cohort 1. MHC-I HC loss thus is heterogeneously manifest across NSCLC patient
319 tumors, and these may develop or progress differently in defined TME regions within individual
320 patients.

321 Given its significant loss in NSCLC, we asked whether tumor cell MHC-I expression may
322 be associated with NK and CD8 T cell infiltrates into the TME. In pairwise Spearman correlations
323 of IHC features across all patient tumors, we found that the density of CD56$^+$ and CD8$^+$ cells
324 significantly correlated with expression levels of both MHC-I HC and β2m in AdenoCA and SCC
325 (**figure 1C,F**). Moreover, CD56$^+$ cells correlated with CD8$^+$ cells, most profoundly in PT regions.

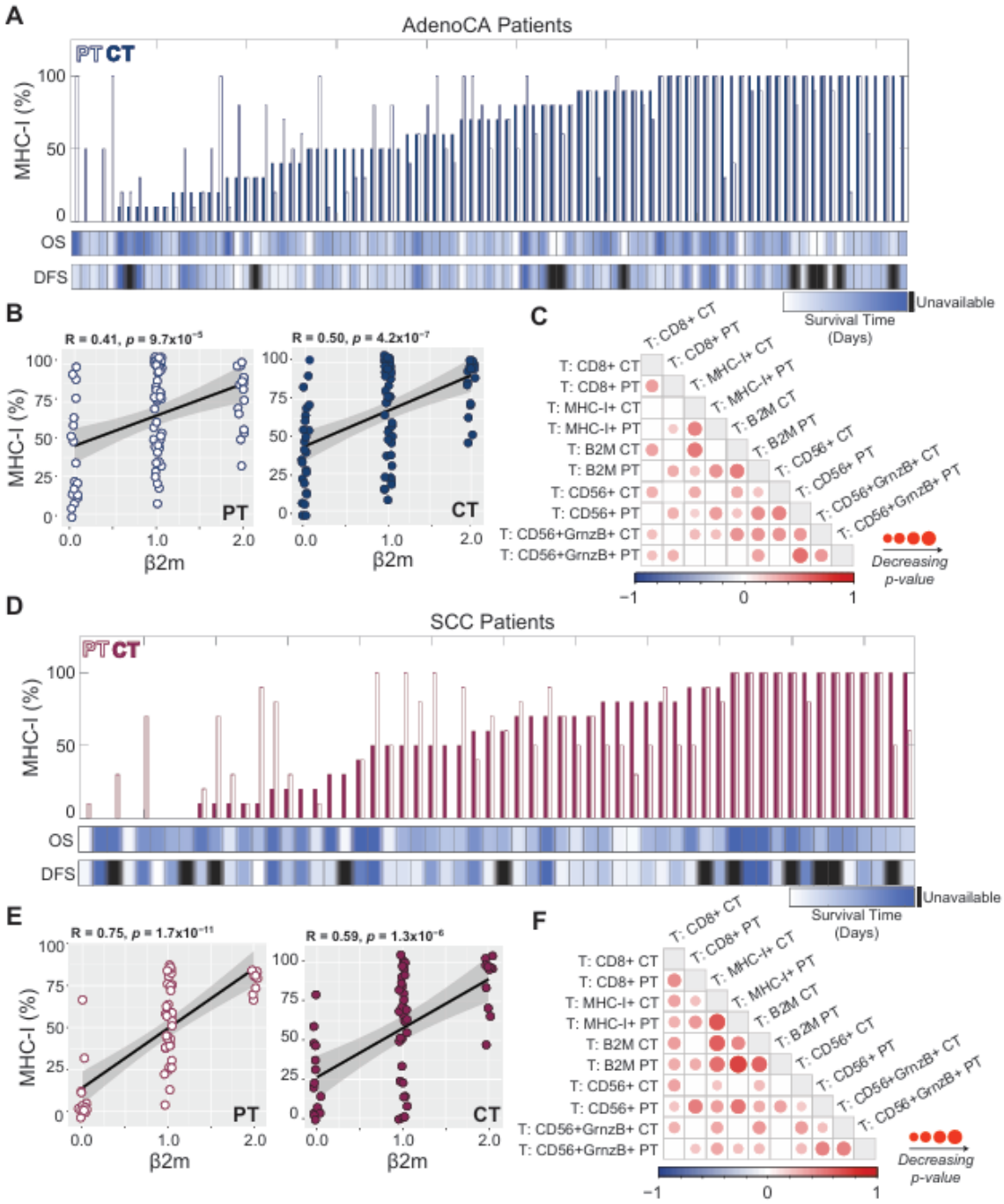

326

327 **Figure 1. MHC-I expression exhibits intra- and inter-tumor heterogeneity and correlates with lym-**
328 **phocyte occupancy. (A&D)** MHC-I is variably expressed in tumors and across AdenoCA **(A)** and SCC **(D)**
329 patients. **(B&E)** β2M expression correlates positively with MHC-I expression in AdenoCA **(B)** and SCC **(E)**.
330 **(C&F)** The heatmaps show Spearman correlations (R) among IHC features in AdneoCA **(C)** and SCC **(F)**.
331 Insignificant correlations (p>0.05) are shaded white; identity correlations are shaded grey.

332 **Concurrent tumor-infiltrating CD8$^+$ and CD56$^+$ immune cells are associated with patient**
333 **survival in human NSCLC independent of MHC-I expression.** Prior work showed that the den-
334 sity of tumor infiltrating CD8 T cells is associated with better patient survival.[15 16] Given MHC-I's
335 effect on target cell recognition by CD8 T cells and NK cells, we asked if MHC-I HC expression
336 was associated with patient outcome. We did not detect any significant association between DFS
337 or OS and MHC-I HC in CT, PT, or averaged across CT and PT (**figure 2A-B, supplemental**
338 **figure S4**). We thus investigated whether densities of intra-tumoral CD8$^+$ or CD56$^+$ cells were
339 associated with DFS or OS outcomes for Cohort 1 patients (**figure 2C-F**). High intra-tumoral
340 CD56$^+$ and CD8$^+$ cell counts averaged across CT and PT were each positively associated with
341 DFS and OS (**figure 2C-F**)**.** Similar trends were observed when considering CT and PT separately
342 (**supplemental figures S5-S6**). Further assessment revealed that simultaneously high CD8$^+$ and
343 CD56$^+$ counts were more strongly associated with prolonged OS (**figure 2H**). Their joint impact
344 on DFS was less striking, but evident when considering density of CD8$^+$ and CD56$^+$ cells in CT
345 only (**figure 2G, supplemental figure S7**). Observations from Kaplan-Meier analyses were con-
346 sistent when adjusting for patient age and sex in a Cox proportional hazards model (HR=0.199,
347 $p<1\text{x}10^{-3}$), and statistical power was insufficient to adjust for cancer stage and prior chemotherapy
348 treatment (**supplemental table 1**). Collectively, these data demonstrate that combined presence
349 of NK cells and CD8 T cells predicts better OS, pointing towards potential complementary anti-
350 tumor activities.

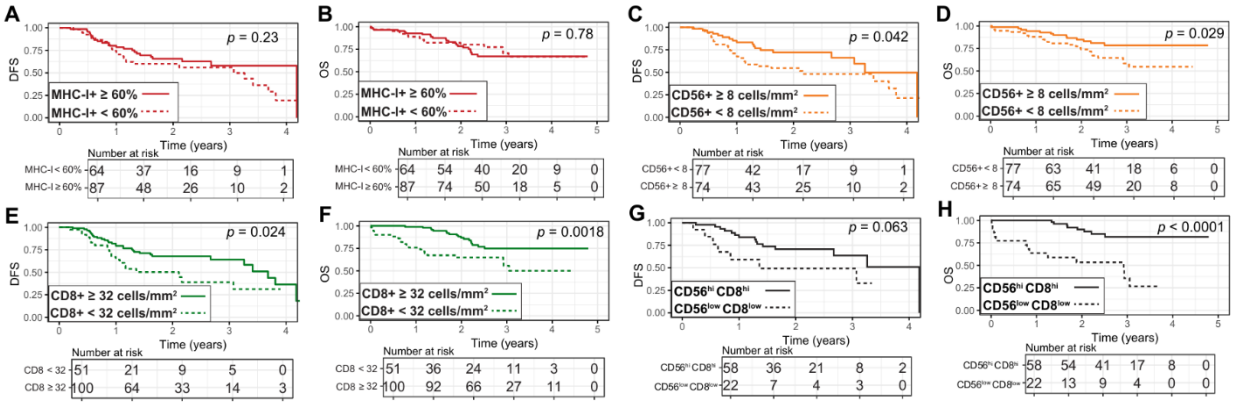

Figure 2. Survival probability increases with increasing CD8⁺ and CD56⁺ lymphocyte infiltrates. Kaplan-Meier analysis predicts DFS or OS with respect to tumor cell MHC-I HC expression **(A&B)**, CD56⁺ cell counts **(C&D)**, CD8⁺ cell counts **(E&F)**, or coincident CD56⁺ and CD8⁺ counts **(G&H)** averaged between CT/PT. *P*-value, log-rank test.

mIF reveals the extent of MHC-I expression variation in patient resected tumor tissues. To further explore the relationship between lymphocyte infiltration and activation and tumor cell MHC-I expression considering its vast heterogeneity in NSCLC and the increased prognostic power observed with simultaneous infiltration of NK cells and CD8 T cells, we implemented mIF imaging with combined spatial analysis of whole tumor sections.

Like the TMA analysis, we observed variable MHC-I HC expression by mIF (**figure 3A**). Because prior work demonstrated that CD8 T cell infiltrations in NSCLC are heterogeneous across tumor regions,[19] we developed a tumor regional approach to delineate spatial relationships between NK cells, T cells and tumor cell MHC-I HC expression (**supplemental figure S1, Methods**). Cohort-wide MHC-I expression per region revealed total MHC-I HC loss in 26% of regions and >90% loss in 47% of regions, with similar distributions observed in AdenoCA and SCC (**figure 3B**). Wide-ranging inter- and intra-patient MHC-I HC expression variability was observed with the mean expression per patient ranging from 0.1%-81% of panCK⁺ cells, and at least one region per tumor displaying >30% loss (**figure 3C**). Tumor cell MHC-I HC loss was thus common among NSCLC patients and heterogeneous across tumor resections.

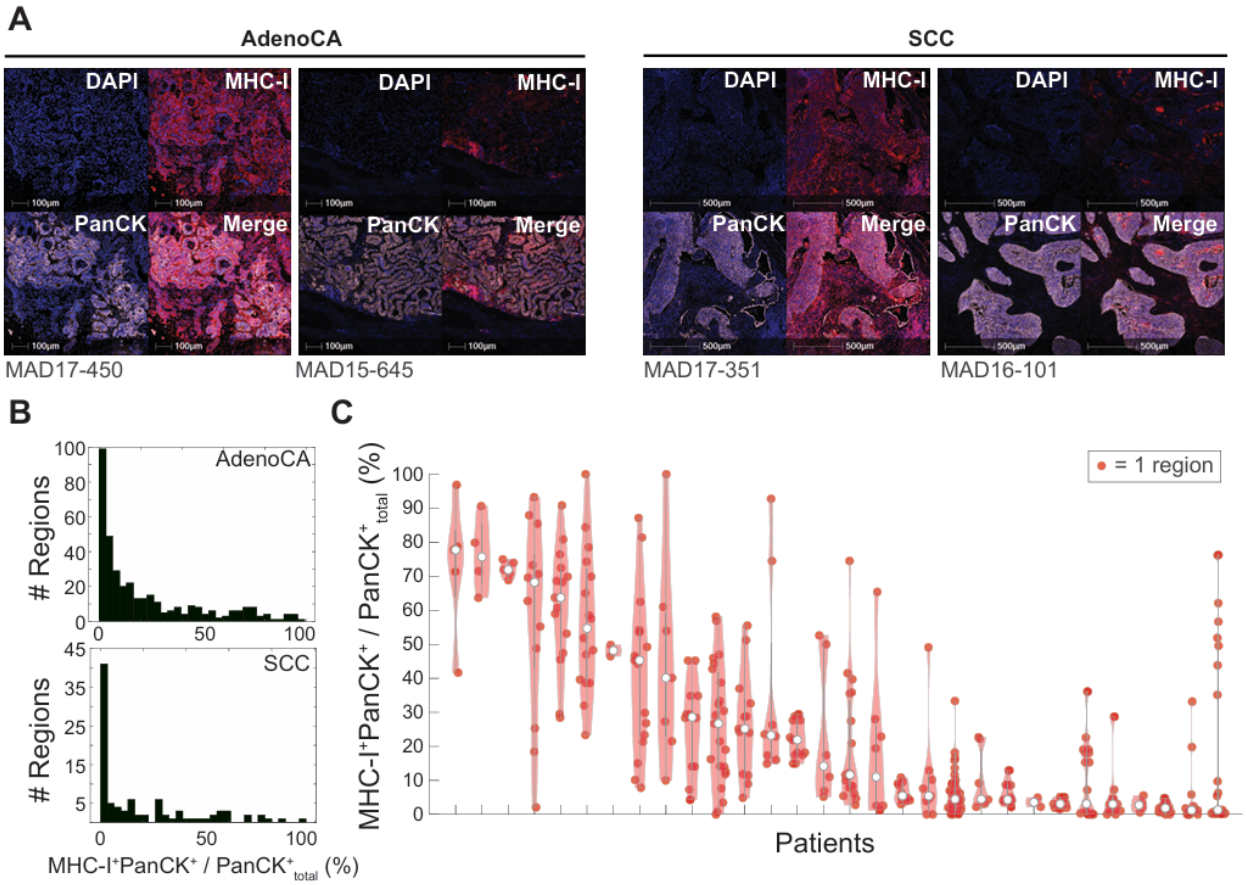

Figure 3. mIF imaging reveals extent of MHC-I HC expression variation in resected patient tumor tissues. (A) Representative images exemplify MHC-I loss in AdenoCA and SCC. **(B)** Histograms of (%) MHC-I$^+$ tumor cells in each region of AdenoCA and SCC. **(C)** The (%) MHC-I$^+$ tumor cells in each region per patient for AdenoCA and SCC.

Tumor cell MHC-I deficiency is associated with decreased NK and T cell presence and activity in the NSCLC TME. We next investigated how NK cell, or CD8 T cell infiltration and activation corresponded to tumor cell MHC-I HC variability by building OPLSDA models to compare the presence of T cells and NK cells in MHC-I-disparate AdenoCA (**figure 4A-D**) or SCC (**figure 4E-H**) tumor regions. Lymphocyte activation was inferred by IFNγ staining in all Cohort 2 resections, though IFNγ is a secreted cytokine and as such its source cannot be definitively determined by mIF. Three tumors displayed strong IFNγ staining in nests lacking substantial lymphocyte infiltration, possibly indicative of a non-lymphocyte source of IFNγ. Nonetheless, in the

383 remaining tumors (n=33) we observed IFNγ predominantly in the presence of NK cells and T cells,

384 indicative of lymphocyte activation (**figure 5, supplemental figure S8**).

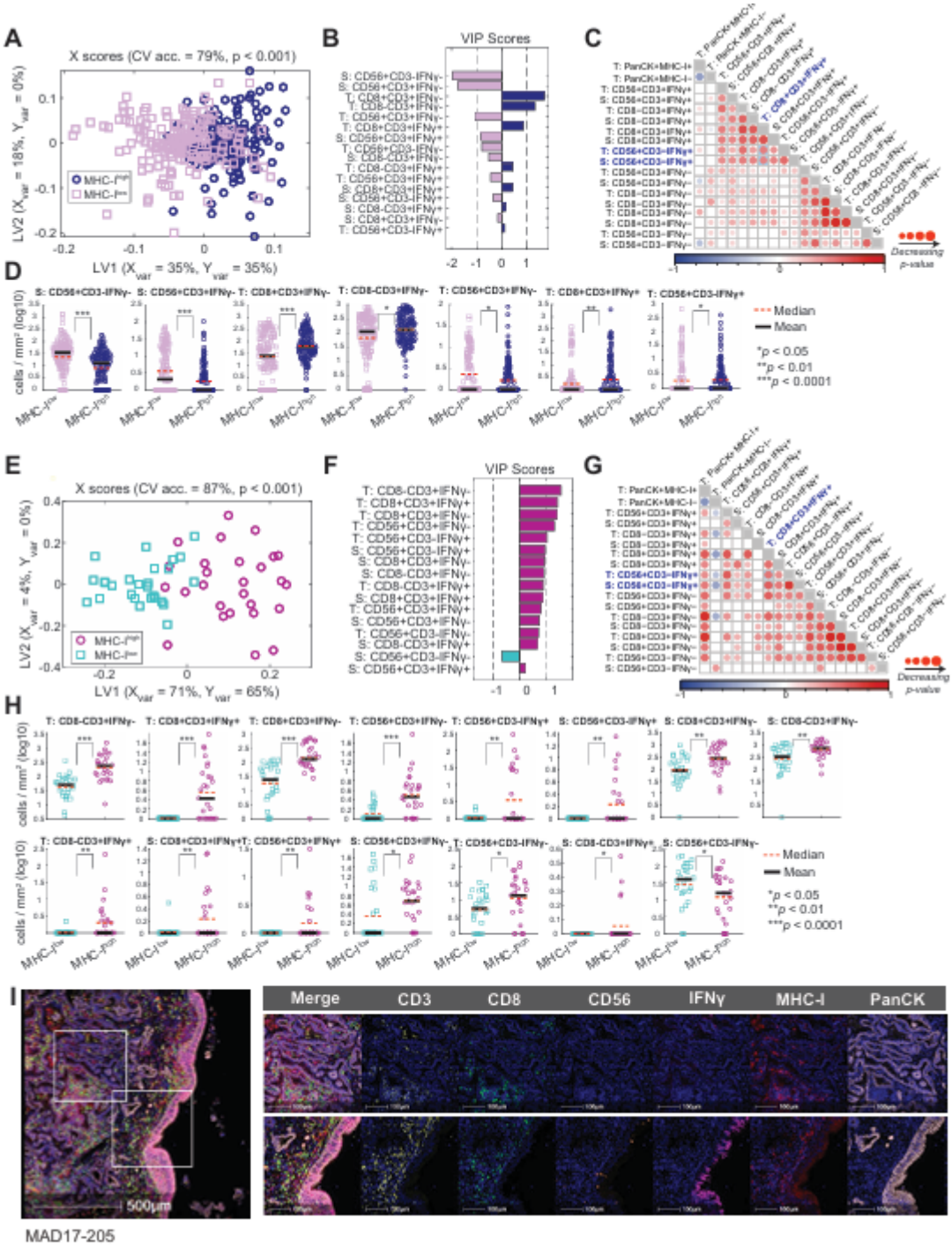

385

386 **Figure 4. Tumor infiltrated lymphocytes and IFNγ expression are associated with high tumor cell**
387 **MHC-I expression.** OPLSDA models discriminate between tumor regions with MHC-I^{+} tumor cell densities
388 (cells/mm^{2}) above or below the median in AdenoCA **(A-D)** and SCC **(E-H)**. CV, cross-validation accuracy.

Significance was determined by a permutation test (p<0.001). **(A&E)** X scores plot, where each point represents one region projected onto latent variables 1 and 2 (LV1&LV2). **(B&F)** VIP scores are shown artificially oriented in the direction of loadings on LV1. |VIP|>1 indicates variables with greater than average influence on the separation between groups. **(C&G)** Spearman correlations among immunologic features in tumor (T) and stroma (S). Insignificant correlations (p>0.05) are shaded white, identity correlations are shaded grey. **(D&H)** Univariate comparisons between model features. Wilcoxon rank sum test with Benjamini-Hochberg correction (*p<0.05; **p<0.01; ***p<0.0001). Only features with p_{adj}<0.05 are shown. **(I)** Representative image shows variation in lymphocyte occupancy and IFNγ staining in MHC-I$^-$ (top) or MHC-I$^+$ (bottom) regions of the same tumor.

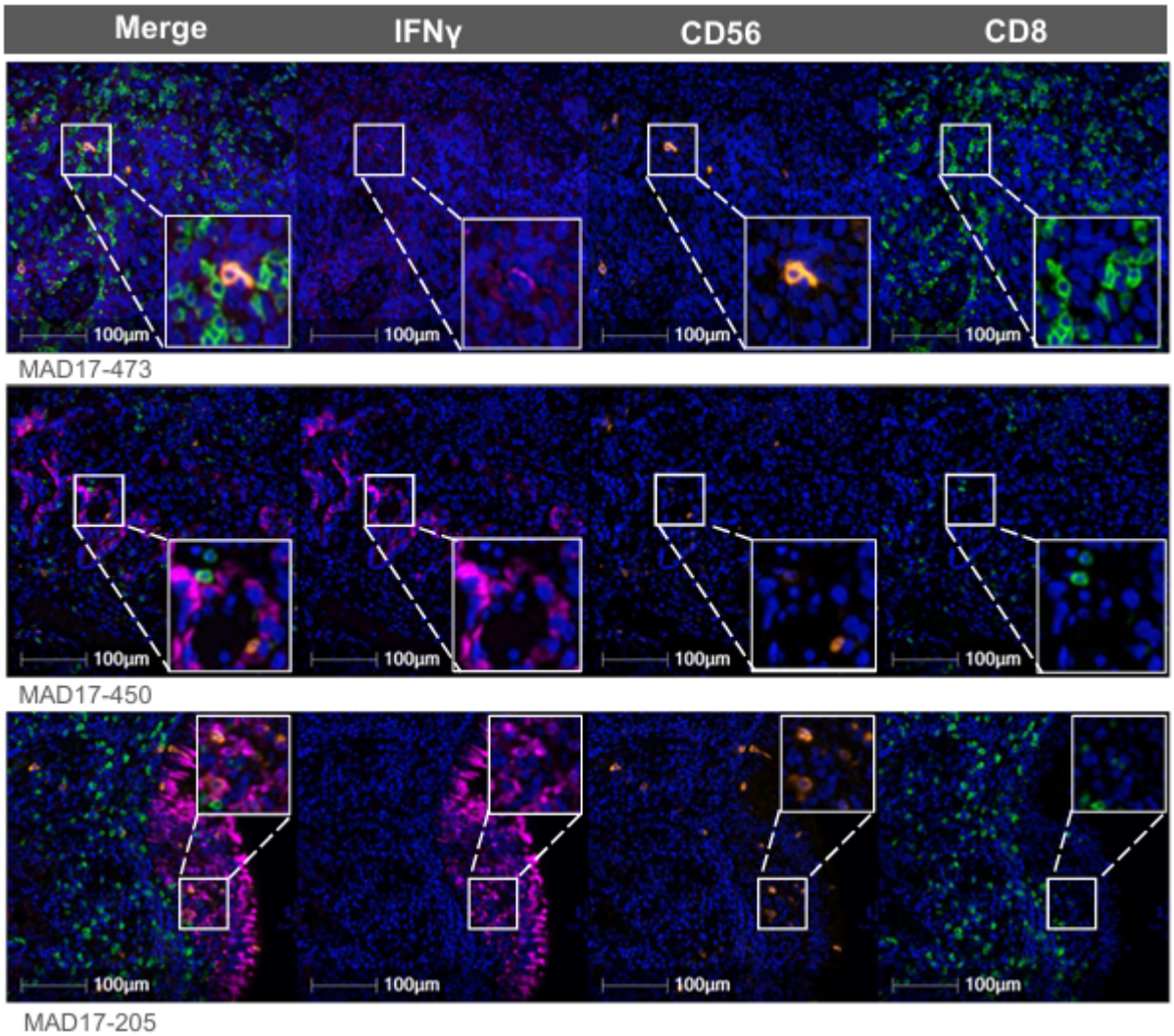

Figure 5. NK cells and CD8 T cells colocalize in areas with IFNγ staining. Representative images show NK cells and CD8 T cells clustered near IFNγ in 3 patient tumors.

The OPLSDA models were able to discriminate between tumor regions with disparate MHC-I expression based on lymphocyte infiltrates with 79% (AdenoCA) or 87% (SCC) accuracy (**figure 4A,E**). VIP scores from the AdenoCA model revealed that stromal CD3$^-$CD56$^+$ NK cells

407 as well as both stroma- and tumor-associated $CD56^+CD3^+$ cells were enriched in tumor regions
408 with tumor MHC-I expression below the median, whereas tumor-associated $CD3^+CD8^-$ (putative
409 $CD4^+$) and $CD3^+CD8^+$ T cells were enriched in regions with MHC-I expression above the median
410 (|VIP|>1) (**figure 4B**). Tumor regions with high MHC-I expression also displayed a greater density
411 of $IFN\gamma^+$ CD8 T cells and NK cells (**figure 4D**), and Spearman correlation analysis revealed that
412 tumoral $IFN\gamma^+$ CD8 T cell densities were positively correlated with $IFN\gamma^+$ NK cells in the stroma
413 and tumor nest (**figure 4C,G**).

414 VIP scores from the SCC model indicated that $CD3^+CD8^-$ and $CD3^+CD8^+$ T cells, $CD3^-$
415 $CD56^+$ NK cells, and $CD56^+CD3^+$ cells were among the top features contributing to the separation
416 between MHC-I replete and deficient tumors (**figure 4F,H**). Akin with the AdenoCAs, the only
417 lymphocyte population found enriched in MHC-I low SCC tumor regions were $IFN\gamma^-$ stromal NK
418 cells. We observed a clear lack of immune infiltration into tumor nests with MHC-I loss in SCC
419 tumors (**supplemental figure S9**). Additionally, we observed significant negative pairwise corre-
420 lations between MHC-I^- tumor cell counts and $IFN\gamma^+$ NK cells, $CD56^+CD3^+$ cells, $CD3^+CD8^+$ T
421 cells, and $CD3^+CD8^-$ T cells, whereas $IFN\gamma^-$ stromal NK cells showed a positive correlation further
422 distinguishing their presence in SCC with MHC-I downregulation (**figure 4G**). Together, these
423 data indicate that IFNγ-expressing NK cells and T cells coinhabited and were associated with
424 tumor regions expressing high MHC-I (**figure 4I**).

425

426 **Local neighborhood analysis of NK cells and CD8 T cells in the TME reveals tightly clus-**
427 **tered lymphocytes marked by IFNγ staining near MHC-$I^{+/-}$ tumor cells.** Given the observed
428 differences in lymphocyte presence in MHC-I-disparate NSCLC tumors, we questioned whether
429 $IFN\gamma^+$ NK cells and CD8 T cells differ from $IFN\gamma^-$ lymphocytes with respect to their proximity to
430 other immune cells and MHC-I expressing tumor cells. To uncover phenotypic differences in cell-
431 cell communication between activated NK cells and CD8 T cells, we determined the cellular

432 neighborhood profile of these effector cell types using spatial, cell-centric analyses of the mIF
433 images (**supplemental figure S2**). The cellular neighborhood profile scores of both tumor- and
434 stroma-associated cells were input into an OPLSDA model to delineate colocalization differences
435 between IFNγ$^{+/-}$ NK cells (**figure 6A-C**) and IFNγ$^{+/-}$ CD8 T cells (**figure 6E-G**). Both models ac-
436 curately distinguished between IFNγ$^{+/-}$ lymphocytes based on their neighborhood profiles with
437 cross-validation accuracy scores of 96% and 97%, respectively (**figure 6A,E**). Comparing the two
438 models, we observed that both IFNγ^{+} NK cells and CD8 T cells associated with all IFNγ^{+} lympho-
439 cyte subsets more than IFNγ^{-} cells (**figure 6B,F**). In agreement with our regional analyses (**figure**
440 **4**), we found that NK cells and CD8 T cells were more likely to be IFNγ^{+} in the tumor as opposed
441 to the surrounding stroma (**figure 6D,H**). Moreover, we observed that IFNγ^{+} NK cells and IFNγ^{+}
442 CD8 T cells in the tumor nests colocalized with MHC-I^{+} tumor cells more frequently than did IFNγ^{-}
443 lymphocytes, suggesting preferential localization of activated cells to tumors with MHC-I expres-
444 sion (**figure 6D,H**). Strikingly, IFNγ^{+} NK cells and CD8 T cells were more frequently associated
445 with MHC-I^{-} tumor cells compared to their IFNγ^{-} counterparts, indicating infiltration of IFNγ-se-
446 creting lymphocytes into both MHC-I^{+} and MHC-I^{-} tumor nests (**figure 6I**). To validate these ob-
447 servations over larger radii, we quantified the number of neighbors <200 μm from a center cell.[35]
448 We observed IFNγ^{+} CD8 T cells had fewer MHC-I^{-} neighbors than MHC-I^{+} neighbors, and their
449 association with MHC-I^{-} tumor cells was less than expected by random chance (**figure 6J**). This
450 may signify deliberate enrichment of IFNγ^{+} CD8 T cells in MHC-I-bearing tumors. In contrast,
451 IFNγ^{+} NK cells associated similarly with MHC-I^{+} and MHC-I^{-} tumor cells, suggesting that NK cells
452 may become or remain activated in the MHC-I-deficient TME. Marked colocalization of IFNγ^{+} NK
453 cells with other IFNγ^{+} lymphocytes including NK cells, CD8^{-} T cells, and CD8^{+} T cells additionally
454 suggests that lymphocytes may be activated *en masse* in MHC-I-bearing tumors. IFNγ produced
455 in these clusters of activated lymphocytes thus may be indicative of type I immune responses in
456 the TME.

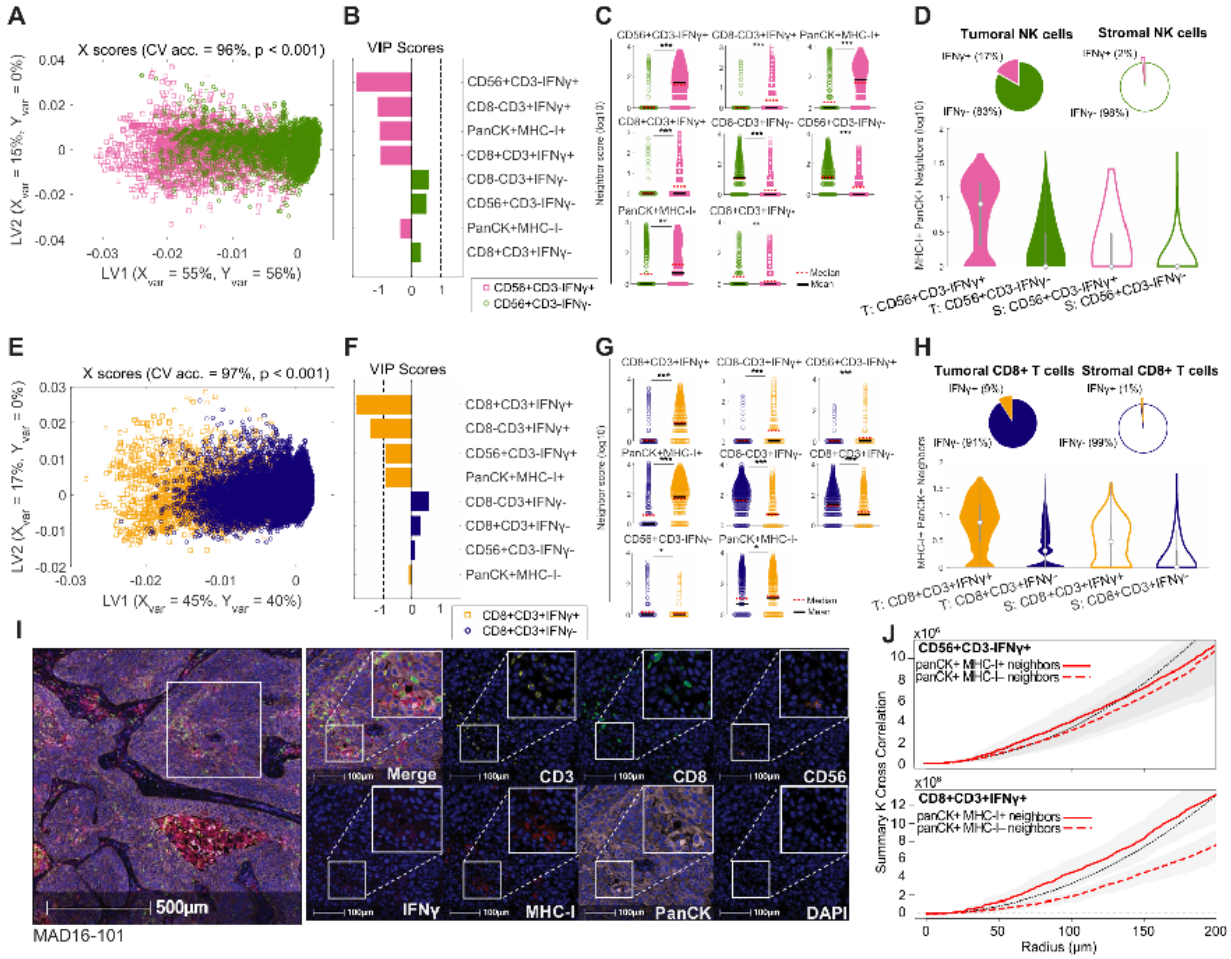

Figure 6. IFNγ⁺ NK cells and IFNγ⁺ CD8 T cells associate with other activated lymphocytes and MHC-I⁺ tumor cells. OPLSDA models discriminate IFNγ$^{+/-}$ NK cells **(A-C)** and IFNγ$^{+/-}$ CD8 T cells **(E-G)**. CV, cross-validation accuracy. Significance was determined by a permutation test (p<0.001). **(A&E)** X scores plot, where each point represents one region projected onto latent variables 1 and 2 (LV1&LV2). **(B&F)** VIP scores are shown artificially oriented in the direction of loadings on LV1. |VIP|>1 indicates a variable with greater than average influence on the separation between groups. **(C&G)** Univariate comparisons between model features. Wilcoxon rank sum test with Benjamini-Hochberg correction (*p<1x10^{-27}; **p<1x10^{-30}; ***p<1x10^{-50}). **(D&H)** The average counts of MHC-I⁺ tumor cell neighbors for IFNγ$^{+/-}$ NK cells **(D)** or IFNγ$^{+/-}$ CD8 T cells **(H)** in tumor (T) or stroma (S) regions. **(I)** Representative mIF image showing a cluster of lymphocytes colocalized with IFNγ in an MHC-I⁻ tumor nest. **(J)** The K function plotted against increasing radii for IFNγ⁺ NK cells and IFNγ⁺ CD8 T cells as the target cell and either MHC-I⁺ (red solid line) or MHC I⁻ (red dashed line) center cells. Grey shading, 95% confidence intervals. Black line, Poisson (null) distribution.

DISCUSSION

While targeting immune checkpoints with CPI has had a substantive impact on the treatment of NSCLC, a minority of patients display durable responses. Whether this is due to hindered immune

475 infiltration, functional exhaustion, tumor cell evasion of immune recognition by loss of MHC-I ex-
476 pression, or alternative mechanisms remains to be determined. Understanding the basis of this
477 selectivity will increase the appropriate targeting of CPI or combination therapies to patients most
478 likely to benefit and will ultimately lead to innovative approaches to expand the proportion of pa-
479 tients who receive clinical benefit.

480 We hypothesized that coordinated activities of both CD8 T cells and NK cells may be
481 needed to mediate lysis of tumor cells while also preventing tumor cell escape via an MHC-I loss
482 mechanism. We analyzed resected patient tumor tissues by both traditional IHC and mIF to sim-
483 ultaneously probe NK cells and CD8 T cells *in situ*, their effector activity indicated by IFNγ staining,
484 and their co-localization in MHC-I HC disparate tumors. To define differences in lymphocyte acti-
485 vation and intercellular communication in MHC-I$^{+/-}$ tumors, we leveraged the inherent heteroge-
486 neity of the TME by developing a suite of spatial analysis methods spanning whole tumors, tumor
487 sub-regions, and single-cell enumeration of NK cell and T cell neighborhoods. This use of inte-
488 grative systems consistently pointed towards coordinated anti-tumor activity of NK cells and T
489 cells, particularly in MHC-I^{+} tumors.

490 Consistent with prior work,[8 11 13] both cohorts displayed stark inter- and intra-tumoral MHC-
491 I expression heterogeneity. Although MHC-I loss can lead to the development of CD8 T cell re-
492 fractory tumors, we did not observe an association between tumor cell MHC-I HC expression and
493 patient survival in this study. Others have speculated cohort-specific composition, clinicopatho-
494 logic characteristics, genetic contribution and/or survival/events may obfuscate any potential as-
495 sociation.[11-13] MHC-I loss thus may indirectly impact patient survival by regulating lymphocyte
496 occupancy and activation.

497 IHC analysis of Cohort 1 revealed that tumors with simultaneously high counts of CD8^{+}
498 and CD56^{+} cells were more strongly associated with OS compared to tumors with high CD56^{+} or
499 CD8^{+} cells only. Positive correlations between CD8^{+} and CD56^{+} cell counts suggests possible

500 intercellular communication playing a role in tumor control. Using mIF to concurrently enumerate
501 NK cell and CD8 T cell infiltrates in Cohort 2, we observed positively correlated tumor-infiltrating
502 NK cells and CD8 T cells with greater densities in tumor nests expressing high levels of MHC-I,
503 indicating coordinated infiltration. Furthermore, spatial analysis of local cellular neighborhoods
504 revealed infiltrated NK and CD8 T cells are present in clusters marked by IFNγ activity together
505 with $CD8^{-}$ T cells. Though much less frequent, similar immune clusters were observed in tumors
506 with MHC-I HC loss, suggesting that an effector response involving NK cells, CD8 T cells, and
507 CD4 T cells can be active, and possibly leveraged, even in a setting considered refractory to
508 lymphocyte immune control.

509 Whether intra-tumoral IFNγ promotes tumor cell MHC-I expression, immune recruitment
510 and colocalization, or coordinated lymphocyte effector activity awaits further analysis, but these
511 findings suggest that CPI plus novel approaches designed to jointly elicit NK and T cell effector
512 activities may be key to developing next generation immunotherapies. Antigen-stimulated NK
513 cells have been shown to provide support to CD8 T cell antitumor immunity in a mouse model of
514 lung adenocarcinoma.[25] Likewise, human induced pluripotent stem cell (iPSC-)derived NK cells
515 have been shown to enhance T cell recruitment and activation to tumors, coinciding with improved
516 T cell sensitivity to CPI and enhanced antitumor control.[38] Cytokine activation can additionally
517 invigorate NK cells to curb or regress tumor outgrowth, even in MHC-I^{-} tumors.[28] The potential
518 benefit of NK cells in NSCLC is bolstered by prior work that showed that human NK cell cytolytic
519 activity is associated with lower cancer risk,[39] whereas NK cell deficiency is associated with in-
520 creased cancer risk.[40-42] Our data contrast recent observations in soft tissue sarcoma that NK cell
521 infiltrates indicate a poor prognosis and do not colocalize with CD8 T cells or MHC-I^{+} tumor cells,
522 indicating that the role of NK cells may be context-specific.[43]

523 Our findings that NK cells infiltrated into tumor nests and displayed evidence of IFNγ ac-
524 tivity in NSCLC begs the question, why might tumoral NK cells become ineffective drivers of anti-

525 tumor immunity? Emerging evidence suggests that NK cell activity may be hindered in the lung
526 cancer TME. Human NKp46^{+} NK cells were shown to infiltrate the invasive margin of lung tissue
527 stroma surrounding tumor nests in NSCLC patients with no apparent effect on clinical outcomes
528 [24]. These intra-tumoral NK cells displayed inferior effector activities in comparison to their coun-
529 terpart NK cells in peripheral blood.[24] Whether due to suppressive mechanisms associated with
530 the lung environment itself[44] or more direct suppression via tumor cells remains unresolved as
531 cancer cells can downregulate or secrete NK receptor ligands to evade natural killing, and the
532 TME is rife with suppressive factors which can impede NK cell activity.[45] Prior work in mouse
533 models has further shown NK cells also undergo disarming in MHC-I^{-} tumors rendering them
534 hyporesponsive and unable to mediate tumor cell clearance.[28 46] As our study affirms the signifi-
535 cant association with survival and notable infiltration into MHC-I^{+} tumor nests of NK cells in
536 NSCLC, future studies are needed to uncover the root causes of NK cell disarming in the lung
537 cancer TME to fully realize their potential as anti-tumor effectors.

538 Though these multifaceted spatial analyses consistently revealed NK cell and CD8 T cell
539 co-occurrence within NSCLC tumors, there are several limitations to consider. The TMA data from
540 Cohort 1 were manually generated by a pathologist, a concern which is mitigated as automated
541 analysis yielded similar results. Cohort 2 was limited by a relatively small sample size, warranting
542 future investigations to verify the associations observed in this study. mIF imaging was limited to
543 six phenotypic markers plus nuclear staining, thus constraining analysis of the full complexity of
544 the tumor-associated immune milieu. Consequently, we relied on IFNγ expression as a marker of
545 lymphocyte activity and were unable to test for expression of other cytotoxic markers and inhibi-
546 tory ligands which may obscure true lymphocyte activity levels. As IFNγ is a secreted cytokine,
547 we were unable to definitively determine its source; however, analysis of our data without three
548 select tumors which displayed strong IFNγ staining in the absence of lymphocytes yielded similar
549 results. The majority of IFNγ staining in the remainder of the cohort was colocalized with a heavy

550 lymphocyte presence. Ongoing work with higher dimensional imaging (e.g., spatial transcriptom-
551 ics) will provide a more comprehensive view of immune cell diversity, occupancy, proliferation,
552 and activation in the TME. Because the cohort was composed of only complete resections, we
553 were unable to assess tissues after chemotherapy or immunotherapy treatment. It remains to be
554 determined whether NK cells drive recruitment and/or activation of CD8 T cells in the TME, or
555 vice versa. Likewise, whether differences in lymphocyte populations and activity in tumors with
556 MHC-I loss results from differences in lymphocyte infiltration, expansion, or retention in the TME
557 remains unclear. Other outstanding questions include whether patient tumors are infiltrated by
558 circulating NK cells with higher baseline cytotoxic activity, by lung resident NK cells with lower
559 baseline cytotoxic activity, or both. Whether these different types of NK cells may affect other
560 tumor-infiltrating immune cells, such as helper T cells or myeloid cells, and whether there are
561 specific interactions that either cause or arise from the spatial associations observed in the data
562 remains to be determined. Future mechanistic studies in animal models will help to delineate the
563 effect of MHC-I on the balance of NK cells and their impact on the tumor-immune landscape.

564 Notwithstanding these challenges, we have shown that tumor cell MHC-I HC loss nega-
565 tively impacted lymphocyte occupancy and activity in the NSCLC TME and that NK cell and CD8
566 T cells jointly infiltrate tumor nests which positively impacts patient survival. This evidence of lym-
567 phocyte activation and intercellular communication in the presence of MHC-I^{+} tumors highlights
568 both the vital importance and promise for developing novel immunotherapies that leverage both
569 NK cells and CD8 T cells to enhance immunologic control of NSCLC.

570

571 **REFERENCES**

572 1. Molina JR, Yang P, Cassivi SD, et al. Non-small cell lung cancer: epidemiology, risk factors,
573 treatment, and survivorship. *Mayo Clinic proceedings* 2008;83(5):584-94. doi:
574 10.4065/83.5.584

575 2. Siegel RL, Miller KD, Fuchs HE, et al. Cancer statistics, 2022. *CA: a cancer journal for clinicians*
576 2022;72(1):7-33. doi: 10.3322/caac.21708 [published Online First: 2022/01/13]

577 3. Chen Z, Fillmore CM, Hammerman PS, et al. Non-small-cell lung cancers: a heterogeneous set
578 of diseases. *Nat Rev Cancer* 2014;14(8):535-46. doi: 10.1038/nrc3775 [published Online
579 First: 2014/07/25]

580 4. Travis WD, Brambilla E, Noguchi M, et al. International Association for the Study of Lung
581 Cancer/American Thoracic Society/European Respiratory Society: international
582 multidisciplinary classification of lung adenocarcinoma: executive summary. *Proc Am*
583 *Thorac Soc* 2011;8(5):381-5. doi: 10.1513/pats.201107-042ST [published Online First:
584 2011/09/20]

585 5. Stankovic B, Bjorhovde HAK, Skarshaug R, et al. Immune Cell Composition in Human Non-small
586 Cell Lung Cancer. *Frontiers in immunology* 2018;9:3101. doi: 10.3389/fimmu.2018.03101
587 [published Online First: 2019/02/19]

588 6. Garrido F, Aptsiauri N, Doorduijn EM, et al. The urgent need to recover MHC class I in cancers
589 for effective immunotherapy. *Current opinion in immunology* 2016;39:44-51. doi:
590 10.1016/j.coi.2015.12.007 [published Online First: 2016/01/23]

591 7. Thunnissen E, van der Oord K, den Bakker M. Prognostic and predictive biomarkers in lung
592 cancer. A review. *Virchows Arch* 2014;464(3):347-58. doi: 10.1007/s00428-014-1535-4
593 [published Online First: 2014/01/15]

594 8. Redondo M, Ruiz-Cabello F, Concha A, et al. Altered HLA class I expression in non-small cell
595 lung cancer is independent of c-myc activation. *Cancer research* 1991;51(9):2463-8.

596 9. Korkolopoulou P, Kaklamanis L, Pezzella F, et al. Loss of antigen-presenting molecules (MHC
597 class I and TAP-1) in lung cancer. *British journal of cancer* 1996;73(2):148-53. doi:
598 10.1038/bjc.1996.28 [published Online First: 1996/01/01]

599 10. Delp K, Momburg F, Hilmes C, et al. Functional deficiencies of components of the MHC class I
600 antigen pathway in human tumors of epithelial origin. *Bone Marrow Transplant* 2000;25
601 Suppl 2:S88-95. doi: 10.1038/sj.bmt.1702363 [published Online First: 2000/08/10]

602 11. Ramnath N, Tan D, Li Q, et al. Is downregulation of MHC class I antigen expression in human
603 non-small cell lung cancer associated with prolonged survival? *Cancer immunology,*
604 *immunotherapy : CII* 2006;55(8):891-9. doi: 10.1007/s00262-005-0085-7 [published
605 Online First: 2005/09/28]

606 12. Li X, Guo F, Liu Y, et al. NLRC5 expression in tumors and its role as a negative prognostic
607 indicator in stage III non-small-cell lung cancer patients. *Oncol Lett* 2015;10(3):1533-40.
608 doi: 10.3892/ol.2015.3471 [published Online First: 2015/12/02]

609 13. Datar IJ, Hauc SC, Desai S, et al. Spatial Analysis and Clinical Significance of HLA Class-I and
610 Class-II Subunit Expression in Non-Small Cell Lung Cancer. *Clinical cancer research : an*
611 *official journal of the American Association for Cancer Research* 2021;27(10):2837-47. doi:
612 10.1158/1078-0432.CCR-20-3655 [published Online First: 2021/02/20]

613 14. Kikuchi E, Yamazaki K, Torigoe T, et al. HLA class I antigen expression is associated with a
614 favorable prognosis in early stage non-small cell lung cancer. *Cancer Sci* 2007;98(9):1424-
615 30. doi: 10.1111/j.1349-7006.2007.00558.x [published Online First: 2007/07/25]

616 15. Geng Y, Shao Y, He W, et al. Prognostic Role of Tumor-Infiltrating Lymphocytes in Lung Cancer:
617 a Meta-Analysis. *Cellular physiology and biochemistry : international journal of*
618 *experimental cellular physiology, biochemistry, and pharmacology* 2015;37(4):1560-71.
619 doi: 10.1159/000438523 [published Online First: 2015/10/30]

620 16. Zeng DQ, Yu YF, Ou QY, et al. Prognostic and predictive value of tumor-infiltrating
621 lymphocytes for clinical therapeutic research in patients with non-small cell lung cancer.
622 *Oncotarget* 2016;7(12):13765-81. doi: 10.18632/oncotarget.7282 [published Online First:
623 2016/02/13]

624 17. Schalper KA, Brown J, Carvajal-Hausdorf D, et al. Objective measurement and clinical
625 significance of TILs in non-small cell lung cancer. *J Natl Cancer Inst* 2015;107(3) doi:
626 10.1093/jnci/dju435 [published Online First: 2015/02/05]

627 18. Esendagli G, Bruderek K, Goldmann T, et al. Malignant and non-malignant lung tissue areas
628 are differentially populated by natural killer cells and regulatory T cells in non-small cell
629 lung cancer. *Lung cancer* 2008;59(1):32-40. doi: 10.1016/j.lungcan.2007.07.022

630 19. Obeid JM, Wages NA, Hu Y, et al. Heterogeneity of CD8(+) tumor-infiltrating lymphocytes in
631 non-small-cell lung cancer: impact on patient prognostic assessments and comparison of
632 quantification by different sampling strategies. *Cancer immunology, immunotherapy : CII*
633 2017;66(1):33-43. doi: 10.1007/s00262-016-1908-4 [published Online First: 2016/10/23]

634 20. Federico L, McGrail DJ, Bentebibel SE, et al. Distinct tumor-infiltrating lymphocyte landscapes
635 are associated with clinical outcomes in localized non-small-cell lung cancer. *Annals of*
636 *oncology : official journal of the European Society for Medical Oncology* 2022;33(1):42-56.
637 doi: 10.1016/j.annonc.2021.09.021 [published Online First: 2021/10/16]

638 21. Guillerey C, Huntington ND, Smyth MJ. Targeting natural killer cells in cancer immunotherapy.
639 *Nat Immunol* 2016;17(9):1025-36. doi: 10.1038/ni.3518

640 22. Malmberg KJ, Carlsten M, Bjorklund A, et al. Natural killer cell-mediated immunosurveillance
641 of human cancer. *Semin Immunol* 2017;31:20-29. doi: 10.1016/j.smim.2017.08.002

642 23. Vivier E, Raulet DH, Moretta A, et al. Innate or adaptive immunity? The example of natural
643 killer cells. *Science* 2011;331(6013):44-9. doi: 331/6013/44 [pii]

644 10.1126/science.1198687 [published Online First: 2011/01/08]

645 24. Platonova S, Cherfils-Vicini J, Damotte D, et al. Profound coordinated alterations of
646 intratumoral NK cell phenotype and function in lung carcinoma. *Cancer research*
647 2011;71(16):5412-22. doi: 10.1158/0008-5472.CAN-10-4179

648 25. Schmidt L, Eskiocak B, Kohn R, et al. Enhanced adaptive immune responses in lung
649 adenocarcinoma through natural killer cell stimulation. *Proc Natl Acad Sci U S A*
650 2019;116(35):17460-69. doi: 10.1073/pnas.1904253116 [published Online First:
651 2019/08/15]

652 26. Liu RB, Engels B, Arina A, et al. Densely granulated murine NK cells eradicate large solid
653 tumors. *Cancer research* 2012;72(8):1964-74. doi: 10.1158/0008-5472.CAN-11-3208

654 27. Nicolai CJ, Wolf N, Chang IC, et al. NK cells mediate clearance of CD8(+) T cell-resistant tumors
655 in response to STING agonists. *Science immunology* 2020;5(45) doi:
656 10.1126/sciimmunol.aaz2738 [published Online First: 2020/03/22]

657 28. Ardolino M, Azimi CS, Iannello A, et al. Cytokine therapy reverses NK cell anergy in MHC-
658 deficient tumors. *J Clin Invest* 2014;124(11):4781-94. doi: 10.1172/JCI74337

659 29. Bottcher JP, Bonavita E, Chakravarty P, et al. NK Cells Stimulate Recruitment of cDC1 into the
660 Tumor Microenvironment Promoting Cancer Immune Control. *Cell* 2018;172(5):1022-37
661 e14. doi: 10.1016/j.cell.2018.01.004

662 30. Kyrysyuk O, Wucherpfennig KW. Designing Cancer Immunotherapies That Engage T Cells and
663 NK Cells. *Annu Rev Immunol* 2023;41:17-38. doi: 10.1146/annurev-immunol-101921-
664 044122 [published Online First: 2022/11/30]

665 31. Erdag G, Schaefer JT, Smolkin ME, et al. Immunotype and immunohistologic characteristics of
666 tumor-infiltrating immune cells are associated with clinical outcome in metastatic
667 melanoma. *Cancer research* 2012;72(5):1070-80. doi: 10.1158/0008-5472.CAN-11-3218
668 [published Online First: 2012/01/24]

669 32. Stam NJ, Spits H, Ploegh HL. Monoclonal antibodies raised against denatured HLA-B locus
670 heavy chains permit biochemical characterization of certain HLA-C locus products. *J*
671 *Immunol* 1986;137(7):2299-306. [published Online First: 1986/10/01]

672 33. Mauldin IS, Mahmutovic A, Young SJ, et al. Multiplex Immunofluorescence Histology for
673 Immune Cell Infiltrates in Melanoma-Associated Tertiary Lymphoid Structures. *Methods*
674 *Mol Biol* 2021;2265:573-87. doi: 10.1007/978-1-0716-1205-7_40 [published Online First:
675 2021/03/12]

676 34. Contal C, O'Quigley J. An application of changepoint methods in studying the effect of age on
677 survival in breast cancer. *Computational Statistics & Data Analysis* 1999;30(3):253-70.
678 doi: https://doi.org/10.1016/S0167-9473(98)00096-6

679 35. Baddeley A, Turner R. spatstat: An R Package for Analyzing Spatial Point Patterns. . *Journal of*
680 *Statistical Software* 2005;12:1-42. doi: doi.org/10.18637/jss.v012.i06

681 36. Dolatshahi S, Butler AL, Siedner MJ, et al. Altered Maternal Antibody Profiles in Women With
682 Human Immunodeficiency Virus Drive Changes in Transplacental Antibody Transfer.
683 *Clinical infectious diseases : an official publication of the Infectious Diseases Society of*
684 *America* 2022;75(8):1359-69. doi: 10.1093/cid/ciac156 [published Online First:
685 2022/03/05]

686 37. Grace PS, Dolatshahi S, Lu LL, et al. Antibody Subclass and Glycosylation Shift Following
687 Effective TB Treatment. *Frontiers in immunology* 2021;12:679973. doi:
688 10.3389/fimmu.2021.679973 [published Online First: 2021/07/23]

689 38. Cichocki F, Bjordahl R, Gaidarova S, et al. iPSC-derived NK cells maintain high cytotoxicity and
690 enhance in vivo tumor control in concert with T cells and anti-PD-1 therapy. *Science*

691 *translational medicine* 2020;12(568) doi: 10.1126/scitranslmed.aaz5618 [published
692 Online First: 2020/11/06]

693 39. Imai K, Matsuyama S, Miyake S, et al. Natural cytotoxic activity of peripheral-blood
694 lymphocytes and cancer incidence: an 11-year follow-up study of a general population.
695 *Lancet* 2000;356(9244):1795-9. doi: 10.1016/S0140-6736(00)03231-1

696 40. Orange JS. Natural killer cell deficiency. *The Journal of allergy and clinical immunology*
697 2013;132(3):515-25. doi: 10.1016/j.jaci.2013.07.020

698 41. Moon WY, Powis SJ. Does Natural Killer Cell Deficiency (NKD) Increase the Risk of Cancer?
699 NKD May Increase the Risk of Some Virus Induced Cancer. *Frontiers in immunology*
700 2019;10:1703. doi: 10.3389/fimmu.2019.01703 [published Online First: 2019/08/06]

701 42. Mace EM, Orange JS. Emerging insights into human health and NK cell biology from the study
702 of NK cell deficiencies. *Immunol Rev* 2019;287(1):202-25. doi: 10.1111/imr.12725
703 [published Online First: 2018/12/20]

704 43. Cruz SM, Sholevar CJ, Judge SJ, et al. Intratumoral NKp46(+) natural killer cells are spatially
705 distanced from T and MHC-I(+) cells with prognostic implications in soft tissue sarcoma.
706 *Frontiers in immunology* 2023;14:1230534. doi: 10.3389/fimmu.2023.1230534
707 [published Online First: 2023/08/07]

708 44. Marquardt N, Kekalainen E, Chen P, et al. Human lung natural killer cells are predominantly
709 comprised of highly differentiated hypofunctional CD69(-)CD56(dim) cells. *The Journal of*
710 *allergy and clinical immunology* 2017;139(4):1321-30 e4. doi: 10.1016/j.jaci.2016.07.043

711 45. Granzin M, Wagner J, Kohl U, et al. Shaping of Natural Killer Cell Antitumor Activity by Ex Vivo
712 Cultivation. *Frontiers in immunology* 2017;8:458. doi: 10.3389/fimmu.2017.00458

713 46. Marcus A, Mao AJ, Lensink-Vasan M, et al. Tumor-Derived cGAMP Triggers a STING-Mediated
714 Interferon Response in Non-tumor Cells to Activate the NK Cell Response. *Immunity*
715 2018;49(4):754-63 e4. doi: 10.1016/j.immuni.2018.09.016 [published Online First:
716 2018/10/18]

717

718